Shifts in dissolved organic matter and nutrients in tundra ponds along a gradient of permafrost erosion

Thomas Pacoureau[1,2,3], Flora Mazoyer[1,2,3], Roxane Maranger[3,4], Milla Rautio[2,3,5], Isabelle Laurion[1,2,3]

[1]Laboratoire de limnologie nordique (LimNord), Centre Eau Terre Environnement, Institut national de la recherche scientifique, Québec QC, G1K 9A9, Canada

[2]Center for Northern Studies (CEN), Université Laval, Québec QC, G1V 0A6, Canada

[3]Interuniversity Research Group in Limnology (GRIL), Département des sciences biologiques, Université du Québec à Montréal, Montréal QC, H2X 1Y4, Canada

[4]Département de sciences biologiques, Université de Montréal, Montréal, QC, H2V 0B3, Canada

[5]Département des sciences fondamentales, Université du Québec à Chicoutimi, Chicoutimi, QC, G7H 2B1, Canada

Corresponding authors: Thomas Pacoureau (email: thomas.pacoureau@gmail.com) and Isabelle Laurion (email: isabelle.laurion@inrs.ca).

Abstract

The accelerated thawing of permafrost in ice-wedge polygonal landscapes results in the formation of shallow ponds, where nutrients and dissolved organic matter (DOM) remain poorly characterized. Over three consecutive summers, water was collected from a series of ponds on degrading syngenetic permafrost, representing the most common geomorphological categories: erosive or stable ice-wedge trough ponds and coalescent polygon ponds. Dissolved organic carbon (DOC) and nutrients were quantified, and DOM was characterized using optical analysis. These ponds were rich in carbon and nutrients, particularly the ice-wedge trough ponds with eroding permafrost. They also exhibited higher concentrations of DOC (+30% on average), total nitrogen (+45%), ammonium (+1135%), and total phosphorus (+54%) in the hypolimnion compared to the epilimnion. DOM was mainly of terrestrial origin (57–75% of total fluorescent DOM), though protein-like fluorescent components increased in ponds colonized by vegetation and cyanobacterial mats. Weather conditions significantly influenced DOC (+26% in a wet and warm year) and DOM composition in summer, with warmer temperatures and higher precipitation enhancing lateral DOM transfer from permafrost soils and promoting contributions from cyanobacterial mats. These findings improve the understanding of Arctic pond biogeochemistry, enabling a more accurate assessment of their potential role in climate feedback mechanisms.

Key words: ice-wedge polygonal tundra, permafrost, ponds, dissolved organic matter, nutrients, biogeochemical shifts, weather effects, stratification, PARAFAC, plant colonization.

1. Introduction

The study of carbon (C), nitrogen (N), and phosphorus (P) in freshwater ecosystems is of paramount importance given their influence on primary production, respiration, and the overall metabolic balance of these systems (Berggren et al., 2007; Wrona et al., 2016; Hamdan et al., 2021). While inventories of C, N and P concentrations and elemental forms in some larger Arctic water bodies exist, small tundra ponds (< 1000 m²) are often overlooked (Antoniades and Douglas, 2003; Rautio et al., 2011; Dranga et al., 2018; Wauthy et al., 2018). Ice-wedge polygons, which cover vast areas in the coastal plains and river deltas of Siberia (Kartoziia, 2019), Alaska (Kanevskiy et al., 2013), and northern Canada (Fortier and Allard, 2004; Kokelj et al., 2014), host numerous small ponds that are highly metabolically active and emit disproportionately high amounts of greenhouse gases relative to their size (Abnizova et al., 2012; Langer et al., 2015; Martin et al., 2018; Coch et al., 2020; Prėskienis et al., 2021). The number of thermokarst ponds has risen in recent decades due to climate change (Raynolds et al., 2014; Jorgenson et al., 2015; Liljedahl et al., 2016), yet the factors driving dissolved organic matter (DOM) and nutrient concentrations in lowland tundra ponds remain poorly characterized.

The development of thermokarst features in ice-wedge polygonal terrains creates a variety of pond morphologies with distinct hydrological and biogeochemical characteristics, often coexisting at small spatial scales (Koch et al., 2014; Lara et al., 2015; Prėskienis et al., 2021). These ponds are typically shallow with high perimeter-to-volume ratios, making them important reservoirs for allochthonous DOM and macronutrients exported from eroding soils and shallow organic layers (Rautio et al., 2011; Vonk et al., 2015; Ma et al., 2019). Since DOM reactivity to microbial and photochemical decomposition depends on its chemical composition (Franke et al., 2012; Kellerman et al., 2015), understanding DOM quality–along with C and nutrient stoichiometry–is crucial for assessing potential shifts in the Arctic C cycle in response to permafrost thaw (Vonk et al., 2015; Maranger et al., 2018). The source of DOM significantly influences its composition (Berggren and del Giorgio, 2015). Allochthonous DOM from soils is generally humic and highly processed, while autochthonous DOM from phytoplankton or plant biomass tends to be richer in protein-like and carbohydrate compounds (Benner, 2003; Chen et al., 2014). Interestingly, permafrost-derived DOM has a distinct signature, being depleted in humic compounds compared to typical soil DOM (Spencer et al., 2015; Wang et al., 2018).

Water column stratification is a key factor influenced by DOM inputs from thermokarst activity, which can impact pond chemistry. Despite their shallow depths, stratification is often observed in thermokarst water bodies with high terrestrial organic matter inputs, leading to the accumulation of macronutrients in

oxygen-depleted bottom waters (Breton et al., 2009; Matveev et al., 2016; Wauthy and Rautio, 2020). However, the effects of stratification on DOM and nutrient dynamics in Arctic ponds are rarely studied (Roiha et al., 2015). If Arctic water bodies, particularly those affected by permafrost erosion, become more persistently stratified–similar to trends seen elsewhere (Niedrist et al., 2018; Pilla et al., 2018)–this could disrupt photochemical and biogeochemical cycles, altering light availability and oxygen levels in tundra ecosystems.

The snowmelt period is critical for transporting organic C and mineral sediments to Arctic surface waters (Lamoureux and Lafrenière, 2014), while in summer, rainfall becomes the primary hydrological input, driving sporadic runoff and the export of dissolved organic carbon (DOC), N, and ions from watersheds (Abnizova et al., 2012; Rioux, 2020). The timing and intensity of precipitation play a key role in determining the types of materials exported: low to moderate rainfall increases the flux of dissolved materials, while intense events favor particulate matter transport (Beel et al., 2021). Late-summer precipitation, when the thawing front is at its deepest and vegetation productivity is at its peak, can enhance the export of terrestrial organic matter to streams and ponds. With Arctic rainfall projected to increase over the next century (Bintanja, 2018), the extent to which these shifts influence C and nutrient dynamics in tundra ponds remains an open question.

In this study, we explored spatial variations in DOM quality and the stoichiometry of C and nutrients across three pond categories in ice-wedge polygonal tundra, defined primarily by differences in permafrost erosion, land inputs, and vegetation colonization. Surface and bottom waters were sampled to measure DOC, DOM absorbance and fluorescence, and the speciation of N and P. DOM quality was also characterized in leachates from potential surrounding sources, including permafrost, active and transient soil layers, tundra plants, brown mosses, and cyanobacterial mats. We hypothesized that (i) DOM and nutrient concentrations would be higher in ponds more affected by permafrost degradation, particularly in bottom waters when stratification occurs, (ii) vegetation colonization would stabilize erosion and alter water chemistry; and (iii) the DOM pool in ponds would shift from resembling permafrost in eroding ponds to resembling primary producers in stabilized ponds. Data were collected over three consecutive summers with varying temperatures and precipitation, allowing us to explore the effects of runoff and increasing permafrost thaw depth on C and nutrient storage in ponds. Our goal was to assess how permafrost degradation and local primary production influence C and nutrient mobilization and DOM composition considering climatic variability. Given the rise in thermokarst ponds due to climate change (Raynolds et al., 2014; Jorgenson et al., 2015; Liljedahl et al., 2016), understanding their response to environmental change is essential for evaluating their role in climate feedback mechanisms (Schuur et al., 2022).

2. Materials and methods

2.1. Study site

The Qarlikturvik Valley is located on Bylot Island (73°09'N, 79°58'W) in the Canadian Arctic Archipelago (Nunavut; **Fig. 1**, left side panel). The climate is characterized by a mean annual air temperature of -14.4°C for the 1995–2018 period, with February (-34.8°C) and July (6.4°C) being the coldest and warmest months, respectively (CEN, 2020). Snow typically covers the ground from early October to early June. Manual records of rainfall collected from June to August between 1995–2018 averaged 77.5 mm, with most of the precipitation occurring in July (36.9 mm on average). Ice-wedge degradation in the valley has resulted in the formation of ponds associated with either low- or high-center polygons. This feature is common in low-relief environments underlain by continuous permafrost, where most of the circumpolar freshwater surface area can be found (Grosse et al., 2013; Muster et al., 2017).

The ponds are scattered along the banks of a proglacial river, on a terrace 3 to 5 meters thick (~20 m above sea level) resulting from the aggradation of Holocene deposits composed of peat mixed with aeolian sands and silts (Fortier and Allard, 2004). Carbon dating of plant remains from basal peat gives an age of ~3700 years BP (Fortier and Allard, 2004). The peaty-loess deposits on the study site have excess pore ice and an organic carbon (OC) content of less than 27% dry weight in the first meter (Prėskienis, 2022). The maximum depth of the active layer in summer has been recorded as varying between 30 and 70 cm (Allard et al., 2024). The valley's polygonal wetlands (~20 km²) were found to store a total of 1.654 Tg C in the top meter of soil, with an estimated OC stock of 82 kg C m^{-2} (Ola et al., 2022). Wet sections of the polygons are dominated by sedges, grasses, and mosses, while drier environments, such as polygon ridges and surrounding tundra, supported more diverse communities, including abundant dwarf shrubs.

2.2. Air temperature and precipitation

Air temperature and precipitation data from the growing seasons of 2017, 2018 and 2019 were analyzed to explore potential inter-annual variability in DOM and nutrient concentrations. Daily average air temperature data (CEN, 2020) were used to calculate cumulative thawing degree-days (°C–days; the sum of all temperatures above 0°C on each date). This index reflects both the duration and magnitude of above-freezing temperatures during the growing season. Precipitation (mm) was recorded daily on a rain gauge installed at the research station (Hellman manual rain gauge, 0.5 mm accuracy and 1.0 mm resolution) from early May to late August. Snowfall was converted into equivalent precipitation (mm) using a snow-to-rain conversion factor of 0.1. Cumulative precipitation and degree-days were calculated to compare the timing and total amounts of rain and heat received at the study site each year.

2.3. Pond classification in ice-wedge polygonal tundra

Three categories of ponds were defined to explore the spatial variability of DOM and nutrients in the limnoscape. Ponds were categorized based on their morphology and level of erosion (**Fig. 1**, right panel):

i. Eroding ice-wedge trough (eIWT) ponds represent an advanced degradation state of ice-wedges, with clear signs of soil erosion on shores mostly lacking emergent vegetation, and dark brown waters. They form around high-center polygons and gradually develop into a network of connected channels.
ii. Stable ice-wedge trough (sIWT) ponds are in the process of stabilization. The degrading ice-wedge is progressively overlaid by eroded peat and lacustrine sediments, making sIWT ponds generally shallower but larger than eIWT ponds due to lateral expansion. The shallowest sections are colonized by sedges and bryophytes. Some sIWT ponds show little evidence of soil erosion before vegetation colonization and are also included in this category.
iii. Coalescent polygon (CP) ponds form from the flooding of depressions caused by ground subsidence. They can be relatively large (typically < 500 m^2), sometimes spanning several polygons, and may overtake previously formed ice-wedge trough (IWT) ponds. CP ponds are characterized by transparent waters, steep shores, and flat bottoms with thick photosynthetic mats, mainly dominated by filamentous cyanobacteria (e.g., Oscillatoriaceae), which contribute significantly to phototrophic productivity (Vézina and Vincent, 1997).

Although common, ponds at the center of individual low-center polygons were not sampled. These ponds are extremely shallow and ephemeral, often disappearing during summer or absent in certain years, depending on precipitation and evaporation.

2.4. Pond sampling

Water samples were collected from ponds during the summer months of 2017, 2018, and 2019 for comprehensive chemical analysis. In 2017 and 2018, 15 ponds (5 eIWT, 5 sIWT, and 5 CP ponds) were sampled between July 20–24 for DOM optical analysis, DOC, iron (Fe), total nitrogen (TN), and total phosphorus (TP). The 2019 campaign, conducted from July 13–18, expanded to 20 ponds (8 eIWT, 6 sIWT, and 6 CP ponds) and included additional aliquots for total dissolved nitrogen (TDN), nitrate (NO_3^-, encompassing NO_3^- and NO_2^-), ammonium (NH_4^+), and phosphate (PO_4^{3-}). Before sample collection, temperature and dissolved oxygen profiles were measured at 10 cm intervals using a ProODO meter (YSI Incorporated, Yellow Springs, OH, USA). Samples were retrieved from ~10 cm below the surface, and in 2019, additional samples were collected from the deepest section of the ponds using a peristaltic pump attached to a laminar sampler (Fig. S3 in Matveev et al., 2019). Samples were stored in polycarbonate bottles. A detailed inventory of samples and analyses is provided in Supplementary **Table S1**.

Aliquots for DOC and DOM optical analyses were filtered through pre-combusted glass fibre filters (grade F, nominal retention of 0.3 µm, Advantec, AMD) using a vacuum of 260 mbar, and stored in pre-combusted amber borosilicate glass vials. For DOC, aliquots were acidified with 32% H_3PO_4 (ACS Reagent grade) to a pH < 2. For TN and TP, unfiltered water was placed in polypropylene tubes and fixed with 30% H_2SO_4 (ACS Reagent grade) to a pH < 2. Aliquots for TDN, NO_3^-, NH_4^+ and PO_4^{3-} were filtered using 0.45 µm polyethersulfone syringe filters and stored in polyethylene bottles without preservatives. For Fe, aliquots were filtered the same way but fixed with HNO_3 (Trace Metal grade, 0.2% final concentration) and stored in polypropylene tubes. Samples for DOC, DOM, TP, TN and Fe were stored in the dark at 4°C, while all other samples were kept frozen until analysis.

2.5. Water chemistry analysis

DOC concentration was measured using an Aurora 1030W TOC analyzer (OI Analytical, College Station, TX, USA) following sodium persulfate digestion (EPA Method 415.1). The concentration was reported in mg L^{-1} with a detection limit of 0.15 mg L^{-1}. TN, TDN, NO_3^-, and NH_4^+ were determined by colorimetry on a QuikChem 8500 automated ion analyzer (Lachat Instruments, Milwaukee, WI, USA). For TN, TDN and NO_3^-, the Griess reaction was used after reduction of NO_3^- to NO_2^- by a copper-cadmium column (EPA Method 353.2), following a potassium persulfate digestion step for TN and TDN samples. NH_4^+ was measured as ammonia using the indophenol method (EPA Method 350.1). Dissolved organic nitrogen (DON) was calculated as TDN minus dissolved inorganic nitrogen (DIN = NO_3^- + NH_4^+). TP and PO_4^{3-} were determined by colorimetry on an Astoria 2 analyzer (Astoria-Pacific, Clackamas, OR, USA), after the reduction of antimony-phospho-molybdate complexes by ascorbic acid (EPA Method 365.3), and following a potassium persulfate digestion step for TP. All results for N and P analyses were reported in µg L^{-1}, with detection limits of 4 µg L^{-1} for TN and TDN, 1.4 µg L^{-1} for NH_4^+, 0.4 µg L^{-1} for NO_3^-, and 0.7 µg L^{-1} for TP and PO_4^{3-}. Fe concentration was measured by ICP-AES on a Varian Vista AX CCD (Palo Alto, CA, USA) and reported in mg L^{-1}, with a detection limit of 0.0007 mg L^{-1}. NO_3^- samples were frequently below the detection limit (10 out of 40 cases); values below the detection limit were replaced with half the detection limit value (0.2 µg L^{-1}).

2.6. Leachates from potential DOM sources

Leachates were produced in the laboratory from materials collected in the field, filtered, and further analysed for DOM optical properties. Soil leachates were prepared from soil cores extracted in July 2016 by Prėskienis (2022). Briefly, seven cores were collected using a core drill at the center of permafrost polygons. The thawed section of the active layer (20–25 cm) was collected separately using a spade. Cores

were stored frozen and then sectioned into three depth intervals: the active layer (10–20 cm below the surface), the transient layer (40–50 cm), and the permafrost (90–100 cm). The sections were thawed at 4°C for 12 hours, then mixed with ultrapure water (v/v 1:5) for 6 hours in the dark at 4°C. The slurries were centrifuged, and the DOM leachates were filtered successively through glass fiber filters (grade D, nominal retention of 2.7 µm, Whatman) and polyethersulfone syringe filters (0.22 µm pore size, Advantec MFS). Leachates from primary producers were prepared from material collected in the field during summer of 2018 or 2022. Terrestrial plants included terminal shoots of *Salix Arctica* and *Cassiope tetragona* prostrate shrubs, a mix of graminoids, *Eriophorum sp.* sedges and *Aulacomnium sp.* mosses. They were dried at the field camp lab and stored dry, except for *Eriophorum sp.*, which were frozen while still moist. Primary producers collected from the ponds included *Drepanocladus sp.* aquatic mosses and cyanobacterial mats, which were rinsed and preserved frozen in Whirl-Pak bags. In the laboratory, dry or thawed material was soaked in jars with Milli-Q grade water (weight/volume ratios available in **Table S2**) for three days in the dark at 4°C. Leachates were then filtered through pre-combusted fiber filters (grade D and F, nominal retention of 2.7 and 0.3 µm, respectively, Advantec, AMD). Optical analyses were immediately performed to minimize losses of the most labile molecules.

2.7. DOM optical analysis

Absorbance measurements were performed on a Cary 100 UV-Vis spectrometer (Agilent, Santa Clara, CA, USA) over a wavelength range of 200 to 800 nm (1 nm increments) in dual-beam mode, with ultrapure water as the blank. Spectral absorbance values were corrected by subtracting the mean absorbance between 790 and 800 nm (a null-point adjustment to correct for residual offsets and scattering losses). The Napierian absorption coefficient at 320 nm (a_{320}, hereafter referred to as CDOM), used as a proxy for the concentration of colored DOM, was calculated as a_{320} (m^{-1}) = 2.303 × A_{320} ÷ l, where l is the cuvette pathlength (m) and A_{320} (dimensionless) is the absorbance at 320 nm. The specific absorbance at 254 nm, calculated as $SUVA_{254}$ (L $mgC^{-1}m^{-1}$) = A_{254} ÷ (DOC × l), served as a proxy for DOM aromaticity (Weishaar et al., 2003). $SUVA_{254}$ values were corrected for samples with Fe concentrations higher than 2 mg L^{-1}, using the equation from Poulin et al. (2014), to prevent overestimation caused by Fe complexation with humic substances. The spectral slope coefficient S_{285} (nm^{-1}), calculated between 275 and 295 nm, was used as a relative index for DOM molecular weight (Helms et al., 2008).

Fluorescence excitation-emission matrices (EEMs) were measured using a Cary Eclipse spectrofluorometer (Agilent, Santa Clara, CA, USA) following the procedure outlined by Stedmon et al. (2003). Fluorescence intensity was measured across excitation wavelengths ranging from 240 to 450 nm (5 nm increments) and emission wavelengths from 300 to 560 nm (2 nm increments). EEMs were pre-processed using the

FDOMcorr toolbox v1.6 in MATLAB (version 2020a, The MathWorks, Ismaning, Germany). Correction steps included the removal of noise below 250 nm excitation, intensity corrections for the instrument, subtraction of the daily ultrapure water blanks from the EEMs, and correction for the inner-filter effect (McKnight et al., 2001). Fluorescence intensity was normalized to the area under the Raman peak of water at 350 nm excitation using empirically determined Raman boundaries (Murphy, 2011). The remaining first order Rayleigh scattering was removed by inserting missing values, and data were interpolated for parallel factor (PARAFAC) modeling (Bahram et al., 2006).

PARAFAC modeling was done with the drEEM v0.6.3 and N-way toolboxes in MATLAB. Model development included 276 pond samples, 35 plant samples, 26 permafrost soil samples, 20 transition layer soil samples, and 28 active layer soil samples, for a total of 385 entries (see supplementary information **Text S1**, **Fig. S1** and **S2** for more details). The final 8-component model explained 99.7% of the fluorescence variability in the dataset. Each fluorescent component was expressed by its maximum intensity F_{max} (in Raman units, or RU), serving as a proxy for the concentration of the component in a given sample. Total fluorescence (F_{tot}), also referred to as FDOM, was calculated as the sum of all maximum intensities (ΣF_{max}). The percent contribution of each component to the sum of maximum intensities was also calculated. The components identified by PARAFAC modeling were matched against 119 validated models from the OpenFluor database (Murphy et al., 2014), using Tucker's congruence coefficient (TCC) thresholds of > 0.95 for excitation and emission (TCC combined > 0.9).

2.8. Statistical analysis

To validate the pond classification used in our statistical analysis (eIWT, sIWT, and CP ponds), a cluster analysis was performed based on the following variables: DOC, TP, TN, a_{320}, F_{tot}, $SUVA_{254}$ and the temperature difference between pond surface and bottom (ΔT). For each pond, surface and bottom values were averaged for each year (except for ΔT), and these summer values were then averaged over the three-year period to minimize noise. An agglomerative hierarchical clustering algorithm was applied using the Euclidean distance metric, after standardizing the data with the "scale" function in R (version v4.3.1, R Core Team, 2024). Clustering was performed using the ''agnes'' function from the *cluster* package (Maechler et al., 2023).

Spearman correlations and pairwise p-values were calculated among N species (TN, TDN, DON, DIN, NO_3^- and NH_4^+) and P species (TP and PO_4^{3-}) in the 2019 dataset using the ''rcorr'' function of the *Hmisc* package (Harrell, 2024) to identify redundant variables. To assess the impact of pond category and sampling depth (2019 dataset) or pond category and sampling year (2017–2019 dataset) on DOM, nutrients, and molar

ratios, two-way mixed measures ANOVAs were conducted using the "anova_test" function in the *rstatix* package (Kassambara, 2023). Degrees of freedom were adjusted with the Greenhouse-Geisser correction to avoid inflated F-ratios when the sphericity assumption was violated (Mauchly's test $P \leq 0.05$). Post-hoc pairwise t-tests with Bonferroni corrections were applied for multiple testing. One pond (BYL128) showed unusually high concentrations at the bottom for most of the variables; given the steep, small hole from which the bottom water was sampled, this pond was considered an outlier and its samples were excluded from the analysis of sampling depth effects.

Two principal component analyses (PCAs) were conducted. The first PCA aimed to identify patterns of DOM quality across pond categories and sampling years using the relative abundance of individual PARAFAC components and qualitative CDOM proxies ($SUVA_{254}$ and S_{285}). This PCA was followed by a permutational multivariate analysis of variance (PERMANOVA), using Euclidean distance as the dissimilarity metric with 999 permutations, to test the effect of pond category or sampling year. Pairwise comparisons among pond categories or years were performed using Bonferroni correction to detect any differences among cluster centroids. To evaluate the homogeneity of group dispersions, a permutational analysis of multivariate dispersions (PERMDISP) was conducted. The second PCA aimed to explore associations between PARAFAC components (in % composition) and leachate sources. All variables were standardized to Z-scores before conducting PCA using the *stats* package or PERMANOVA using the *vegan* package (Dixon, 2003).

3. Results

3.1. DOM properties among pond categories, depths, and source leachates

The dendrogram (**Fig. S3**) reveals clusters consistent with the pre-established pond categories. Average values for DOC, CDOM, and FDOM differed among pond categories and sampling depths, with a significant interaction between these two factors. Meanwhile, average $SUVA_{254}$ values differed only according to pond category (**Table S3**). On average, higher DOC was observed in the hypolimnion of eIWT ponds compared to sIWT and CP ponds (**Fig. 2a**). DOM was also more colored and fluorescent in eIWT ponds compared to sIWT and CP ponds (**Fig. 2b** and **c**). Variability in DOC, CDOM, FDOM, and $SUVA_{254}$ was particularly low in CP ponds. In terms of vertical structure, average DOC, CDOM, and FDOM were consistently higher in the hypolimnion of eIWT ponds than in surface waters (**Fig. 2a**, **b**, and **c**). A similar trend was observed in sIWT ponds for DOC (**Fig. 2a**), reflecting the distinct vertical structure among pond categories (**Fig. S4**). All IWT ponds were stratified, and several experienced hypoxia in the bottom layer,

with the patterns being more pronounced in eIWT ponds. In contrast, CP ponds were well-mixed and oxygenated, with dissolved oxygen consistently above 9.7 mg L^{-1} throughout the measurement period.

PARAFAC analysis identified eight components, half of which are commonly reported in aquatic environments and are typically associated with humic-like terrestrial fluorescence (HT1, HT2, HT3 and HT4). Two components exhibited features of humic-like microbial compounds (HM1 and HM2), while two were protein-like compounds, with P1 and P2 being characteristic of tryptophan-like and tyrosine-like fluorescence, respectively (**Table 1**). A detailed description of these components, based on related studies in OpenFluor, is available in supplementary **Text S2**. Overall, DOM in the studied ponds was primarily of terrestrial origin, with humic-like compounds (HT) accounting for 57–75% of total FDOM (**Fig. S5**). Ordination analysis revealed distinct patterns in DOM composition among pond categories (**Fig. 3a**; PERMANOVA, $P < 0.001$), with eIWT, sIWT, and CP ponds forming three distinct clusters (pairwise PERMANOVA comparisons, *P*-adjusted < 0.005). PC1 (52.9% of the variance) grouped samples according to DOM aromaticity ($SUVA_{254}$) and the relative contribution of humic-like compounds (HT1–3; **Fig. 3a** and supplementary **Table S4**). DOM in sIWT ponds displayed intermediate characteristics between eIWT and CP ponds, with CP ponds being characterized by higher proportions of small protein-like molecules (P1%, P2%, high S_{285}, low $SUVA_{254}$) and the humic-like microbial compound HM1.

Using leachates from potential DOM sources, we were able to further characterize the components identified by PARAFAC analysis (**Table 1**). No component was specific to a single leachate, but some components were characteristic of certain sources (**Fig. 4** and **Table S5**). Spectroscopic analysis revealed that the humic-like components HT1–3 were primarily associated with soil leachates. The sum of their contributions to total FDOM ranged from 62 to 76% for active layer leachates, 59 to 78% for transition layer leachates, and 22 to 76% for permafrost leachates. The component HM2 was more abundant in transition layer (5.4 to 9.2% of total FDOM) and permafrost leachates (6.6 to 13%), while HT4 and HM1 were more abundant in cyanobacterial mats (18 to 51% for HT4 and 5.4 to 10% for HM1) and active layer leachates (4 to 12% for HT4 and 5 to 11% for HM1). The two protein-like components P1 and P2 contributed 0–5.1% and 28–91% of total FDOM in plant leachates, and 17–23% and 28–51% in cyanobacterial mat leachates, respectively. While PC1 (54% of the variance) and PC2 (26% of the variance) helped distinguish soil, cyanobacterial mat, and active layer leachates from other sources, PC3 (9.5% of the variance; **Fig. S5**) clearly separated grasses (*Eriophorum* spp. and graminoids) and mosses (aquatic brown mosses and terrestrial mosses), which were characterized by a higher percentage of tryptophan-like component P1, from dwarf shrubs (*Cassiope tetragona* and *Salix arctica*), which were characterized

by a higher percentage of tyrosine-like component P2 (although permafrost leachates also contained a notable amount of P2).

3.2. Nutrient composition among pond categories and depths

The average TN concentration was 1067 ± 36 μg L^{-1}, with DON constituting the dominant fraction of the TN pool, averaging 96.7%. NH_4^+ dominated the DIN fraction (71.7 ± 14.1 μg L^{-1} on average, ~93%), while NO_3^- represented only 6.6% of the DIN on average (2.2 ± 0.4 μg L^{-1}). Further statistical analysis focused on TN, which was strongly correlated with TDN and DON ($\rho > 0.80$, $P < 0.001$), and NH_4^+. Both TN and NH_4^+ concentrations differed among pond categories and sampling depths, with a significant interaction between these two factors (**Table S3**). In eIWT and sIWT ponds, the hypolimnion was enriched in TN compared to the epilimnion, with average concentrations being 1.5 and 1.2 times greater, respectively (**Fig. 5a**). The same pattern was observed for NH_4^+, with average concentrations in the hypolimnion of eIWT and sIWT ponds being 12 and 9 times higher than at the surface, respectively (**Fig 5b**).

The average TP concentration was 36.6 ± 3.4 μg L^{-1}, with ~20% represented by PO_4^{3-} (7.4 ± 1.1 μg L^{-1}). TP concentrations differed by pond category and sampling depth, with a significant interaction between these two factors, while PO_4^{3-} was only affected by pond category (**Table S3**). Average TP concentration in the hypolimnion of eIWT and sIWT ponds was about 2 times higher than in the epilimnion. The bottom waters of eIWT had significantly higher TP compared to the bottom waters of other pond categories (**Fig 5c**). PO_4^{3-} concentrations were, on average, higher in eIWT ponds than in sIWT and CP ponds at the surface, and also higher in eIWT ponds compared to CP ponds at the bottom (**Fig 5d**).

3.3. Interannual variability in thawing degree-days and precipitation

There were marked differences in cumulative thawing degree-days and precipitation among the three growing seasons. Thawing degree-days accumulated earlier in 2019 than in the previous two years (**Fig. 6a**). By the end of the 2019 sampling period (July 18), 256°C–days had been recorded, compared to 229°C–days in 2018 (July 24) and 199°C–days in 2017 (July 21). Although rainfall from June to August was below the 1995–2018 average, 2019 still received more precipitation than the two previous years (**Fig. 6b**). By the end of the sampling period in 2019, a total of 51.4 mm of rain had fallen, compared to 27.6 mm in 2018 and 10.3 mm in 2017. The weather conditions in 2019 were responsible for the observed increase in active layer depth and temperature, with an average increase of 1.9°C at 5 cm depth (1.6°C at 10 cm depth) from May to July, compared to the same period in 2017 and 2018 (CEN, 2020).

3.4. Interannual trends in DOM, TN, and TP

Average surface values of DOC, TN, TP, and elemental ratios in the ponds are summarized in **Table 2**. Results of the ANOVA, assessing the effects of pond category, sampling year, and their interaction, are presented in **Table S6.** Average DOC concentrations were significantly higher in 2019 than in 2017 and 2018 (pairwise t-test, $P < 0.05$). In contrast, average TN was slightly lower in 2018 than in 2017 and 2019 ($P < 0.05$). No differences were observed for mean TP concentrations across the years. Given the variability of carbon and nutrient concentrations among pond categories (DOC and TP) and across years (DOC and TN), we examined the influence of these factors on the carbon-to-nutrient molar ratios. Since nutrient concentrations were relatively high across all samples, the C:N and C:P ratios were generally low (**Table 2**). The higher DOC concentrations in 2019 resulted in higher DOC-to-nutrient ratios overall ($P < 0.05$), whereas no difference was observed between years for the N:P ratio.

Ordination analysis revealed distinct patterns in DOM composition among the years (**Fig. 3b**; PERMANOVA, $P < 0.001$), with 2019 forming a distinct cluster relative to 2017 and 2018 (pairwise PERMANOVA comparisons, *P*-adjusted < 0.005). According to PC2 (18.9% of the variance), DOM in 2019 was characterized by a higher contribution of humic-like compounds HT4 and HM2, a lower contribution of HT3, and was less aromatic (lower $SUVA_{254}$) compared to the two previous years (**Fig. 3c** and **Table S4**).

4. Discussion

4.1. Ponds on the ice-wedge polygonal landscape are DOC- and nutrient-rich ecosystems

In Arctic ponds and lakes, DOC concentration can vary regionally according to factors such as topography, permafrost extent, ground ice content, type of deposits, soil organic carbon content, and vegetation types in the catchment area (Sobek et al., 2007; Coch et al., 2019; Tank et al., 2020; Stolpmann et al., 2021). As in other regions, DOC also depends on water retention time (Catalán et al., 2016; Sobek et al., 2007) and evapoconcentration, as observed in Greenland lakes (Anderson and Stedmon, 2007). In the present study, DOC concentrations (median 18.5 mg L^{-1}, range 10.4 - 32.3 mg L^{-1}; **Fig. 2a**) were at the higher end of the range typically reported for water bodies in the Canadian permafrost region. For example, Stolpmann et al. (2021) reported a median of 2.9 mg L^{-1} for DOC in lakes of Nunavut (n = 302), with a maximum of 31.9 mg L^{-1}. The higher concentrations in our study are likely due to the small size and active thermokarst processes, which can enhance DOC release to ponds through thawing and leaching.

Total nutrient concentrations in these small water bodies were also high (**Fig. 5a** and **c**), a trend further supported by stoichiometric ratios (**Table 2**). This is likely due to their strong connection with the surrounding terrestrial environment, which includes wetlands and thermokarstic erosion. TN concentrations (median 1006 µg L^{-1}, maximum 1831 µg L^{-1}) were consistent with the nutrient levels

observed in shallow water bodies of the Canadian Archipelago (Lim et al., 2001; Antoniades and Douglas, 2003) and thaw ponds on the Arctic Coastal Plain of Alaska (Koch et al., 2014). However, the relative bioavailability of these nutrients is likely to be low, as they are potentially strongly bound to humic DOM. Given the interconnection between the N and C cycles, DON is likely to be of terrestrial origin (as described below) and to have undergone extensive reprocessing (Tremblay and Benner, 2009; Sipler and Bronk, 2015; Kothawala et al., 2021). In contrast, P is either of mineral origin or bound to iron hydroxides (Maranger and Pullin, 2003).

The study site is a major nesting area for snow geese during the summer (Reed et al., 2002). Previous studies have indicated that nutrient concentrations tend to be higher in ponds and lakes frequented by geese (Côté et al., 2010). These waterfowl inputs–whether direct or indirect via terrestrial fertilization–may contribute to the observed nutrient levels (Van Geest et al., 2007; Mariash et al., 2018). However, a more systematic investigation is needed to confirm their influence. Although the C:N molar ratios of the ponds in this study are consistent with those found in other thermokarst systems in the Arctic (**Fig. S7**; Arsenault et al., 2022), the notably lower C:N ratios and higher N:P ratios observed here differ from those found in freshwater systems in other regions, such as lakes in southern Canada (Dupont et al., 2023). Interestingly, the C:P ratio in our ponds aligns with the findings of the aforementioned study. The presence of thick cyanobacterial mats in some of these ponds (Vézina and Vincent, 1997) suggests a potential source of N through biological fixation. However, the extent of N input via this process remains uncertain in thermokarst-influenced systems, where cyanobacterial mats are less prominent and are primarily observed in CP ponds. Regardless of the nutrient sources, N appears to be relatively abundant in Arctic ponds, with unique C:N:P stoichiometries suggesting a distinct N signature in these ecosystems compared with other freshwater systems. This underexplored aspect could be further investigated through stable isotope analysis and biological assays, focusing on changes in N-associated molecular formulae of DOM, amino acid composition, and their persistence in these ecosystems (Cherrier and Bauer, 2004; Ianiri and McCarthy, 2023; Broek et al., 2023).

4.2. Solute patterns along an erosion–stabilization sequence

Our results show that permafrost thaw and soil erosion release substantial amounts of DOM into the eIWT ponds. As the vegetation stabilises the banks in sIWT ponds, DOC concentrations decline (**Fig. 2a** and **Fig. 4a**). In contrast, CP ponds, which are disconnected from the trough network (and thus from soil erosion inputs) and isolated from hydrological inputs during the summer, exhibit significantly lower DOC concentrations (**Fig. 2a**). These well-mixed, shallow systems are likely efficient at photomineralizing the

small DOM pool entering from the catchment, due to the high exposure of their water column to UV radiation (light profiles are available in Mazoyer, 2023).

The dominance of humic-like compounds (HT and HM) in the DOM pool indicates that most of the organic matter in these ponds has a terrestrial origin. These more condensed molecules contain a large number of aromatic rings, typical of humic substances that have undergone extensive microbial processing and humification in soils over long residence times (Kothawala et al., 2021). The terrestrial signature of DOM in these ponds aligns with the findings of Wauthy et al. (2018), who reported similar patterns in systems with degrading permafrost in their catchments. A more detailed comparison with the leachate data further suggests that DOM in eIWT ponds primarily originates from the active and transient layers rather than from permafrost. Specifically, the DOM from these layers and eIWT ponds is strongly associated with humic-like components HT1, HT2, and HT3 (**Fig. 3a** and **4**), indicating that erosion predominantly releases material from more recent layers. The more humified nature of DOM leached from the active layer could be attributed to the seasonal freeze-thaw cycle, which facilitates annual microbial processing of organic material.

As ponds stabilize and vegetation cover increases, the composition of DOM shifts, with a growing contribution of protein-like components in sIWT and CP ponds (**Fig. 3a** and **S4**). This shift indicates a transition in DOM sources, from predominantly allochthonous (derived from surrounding soils) to more autochthonous (produced by primary producers). The increasing contribution of protein-like components P1 and P2 (**Fig. 4**) is likely linked to the growing role of cyanobacterial mats, mosses, and aquatic plants, which gradually colonize the ponds as they become more transparent. This process is also accompanied by an increasing presence of the component HM1 in sIWT and CP ponds (**Fig. 3a**). This humic-like microbial component was reported by Bittar et al. (2015) and linked to the production by the freshwater cyanobacterium *Microcystis aeruginosa*, a species found in thermokarst lakes of Yakutia (Kopyrina et al., 2020). Its association with leachates from cyanobacterial mats in our study (**Fig. 4** and **S5**) suggests that periphytic filamentous species from the Oscillatoriaceae family, commonly found in these mats (Vézina and Vincent, 1997), could release HM1 into pond water. The establishment of vegetation can occur rapidly after the formation of thaw ponds, within a decade according to Magnússon et al. (2020), stabilizing permafrost erosion and shifting DOM composition in ponds, with consequences for its microbial and photochemical mineralization.

4.3. Solutes influenced by stratification

The stratification observed in ice-wedge trough ponds, particularly in eIWT ponds, plays a significant role in the distribution of solutes, as evidenced by the enrichment of DOC, TN, NH_4^+ and TP in the hypolimnion compared to the epilimnion (**Fig. 2a** and **5a**, **b**, and **c**). These ponds remain stratified for much of the open-water season (Prėskienis et al., 2021), with only the upper portion of the water column mixing on a daily basis (unpubl. data). This stratification creates favorable conditions for solute accumulation in the deeper, colder, darker, and hypoxic layers, where microbial and photochemical processing of DOM and nutrients may be slower. In the hypolimnion, NH_4^+ can accumulate due to several factors. First, it may diffuse from nutrient-rich sediments or be laterally transferred from thawing permafrost, a mechanism observed in other systems (Beermann et al., 2017). Syngenetic permafrost, which is rich in organic material (≥12%), has the potential to store large amounts of NH_4^+, and thawing permafrost combined with an expanding active layer has been linked to an increase in NH_4^+ availability in surface waters (Fouché et al., 2020). As in other Arctic water bodies, DIN concentrations in Bylot ponds are relatively low, particularly NO_3^- (Lim et al., 2001), suggesting that the dominant forms of N entering the system are more closely associated with DOM. The low concentrations of DIN are likely driven by mineralization processes, with the produced DIN rapidly consumed or recycled into DON.

The observed increase in TP in the hypolimnion of IWT ponds (approximately twice the surface concentration, **Fig. 5c**) is likely a result of inputs from eroding permafrost soil and proximity to the sediments. As in other Arctic regions (Lim et al., 2001; Koch et al., 2014), PO_4^{3-} concentrations remain relatively low (**Fig. 5d**), which could be due to its complexation with DOM. In these ponds, Fe concentrations are particularly high (on average, 4.5 and 2.3 mg L^{-1} in eIWT and sIWT ponds, respectively, for pooled surface and bottom samples). Elevated Fe may promote the sorption of phosphate to hydrous Fe complexes, a process known to regulate inorganic P availability in the water column (Maranger and Pullin, 2003; Sundman et al., 2016). This complexation could explain the higher TP concentrations observed in the anoxic bottom waters, where P can be released from sediments in the absence of oxygen.

Treating northern ponds and shallow lakes as fully mixed systems can lead to an underestimation of their DOC and nutrient stocks when only surface samples are considered. Just as local-scale heterogeneity in Arctic tundra soils can influence regional-scale carbon dynamics (Lara et al., 2020), we argue that a fine-scale analysis of heterogeneity within Arctic ponds is critical for improving predictions of biogeochemical changes in the polygonal tundra. By considering both surface and bottom samples, we can better understand the potential shifts in nutrient cycling and carbon storage in response to climate change and permafrost thaw.

4.4. Biogeochemical implications

Differences in DOM composition and nutrient concentrations in the water column of tundra ponds likely lead to variable rates of carbon processing (Mostovaya et al., 2016) and fate (respiration versus bacterial production; Allesson et al., 2020). In eIWT ponds, which are particularly rich in humic-like fluorophores and highly stratified, the bottom water remains below 4°C and in darkness for most of the open-water season. With most N and P bound to organic matter, microbial activity is likely limited. However, the complex morphology of these systems creates shallow zones with warmer, more oxygenated, and brighter habitats that should not be overlooked when assessing carbon processing (see bathymetric maps of these ponds in Fig. S2 of Prėskienis et al., 2024). Humic-like compounds are abundant and sensitive to photochemical alterations due to their efficient absorption of sunlight (Murphy et al., 2018). Partial photooxidation of DOM was particularly effective at the surface of Bylot ponds (Laurion and Mladenov, 2013), but did not promote CO_2 production in July (i.e., no DOC loss), potentially due to a seasonal depletion of photoreactive molecules at the surface following a dry period. Therefore, seasonal changes in DOM (and nutrients) and their influence on bacterial production should also be considered in these small water bodies, which are likely responsive to rain events.

As demonstrated in this study, leachates from shrubs (*Cassiope* and *Salix* spp.) are characterized by a high content of protein-like compounds (tyrosine-like amino acids). Previous studies have shown that these protein-like components are leached from Arctic plants (Allain et al., 2023) and are associated with biolabile DOC (Textor et al., 2019). Since shrub growth is increasing in many regions of the circumpolar Arctic (Mekonnen et al., 2021), further research should investigate the potential role of vegetation inputs (shrubs, but also brown mosses and grasses) on permafrost C mineralization, specifically the interaction of DOM pools of different reactivity (i.e., the priming effect).

The ponds studied here presented higher concentrations of DOM and nutrients compared to nearby thermokarst lakes, whether formed in buried glacier ice or ice-wedge polygon terrain (Prėskienis et al., 2021; Coulombe et al., 2022). These ponds may act as a source of C, N, and P that flow downslope into lakes. In a study by Coch et al. (2020), degrading ice-wedge polygons were found to increase DOC concentration in the upper reach of streams in the catchment, though water quality (defined by concentrations in DOC, TDN, and suspended sediment) was not significantly affected at their outflow and was primarily influenced by catchment size. When the hydrological connectivity between disturbed permafrost areas and downstream aquatic systems was high, solute export was found to increase (Lafrenière and Lamoureux, 2013). These studies suggest that degrading permafrost features can influence downstream aquatic systems in Arctic watersheds, depending on the hydrological context (e.g., water

retention time and slope). Studies coupling water quality to hydrology are essential for modeling the effects of permafrost degradation on lateral geochemical fluxes in Arctic catchments.

4.5. Potential effect of climate-driven changes

High-latitude freshwater ecosystems are already responding to rapid climate warming in various ways (Vonk et al., 2015; Saros et al., 2023). Alongside rising temperatures, climate models predict an increase in precipitation at northern latitudes during this century (Bintanja, 2018). Our results suggest that runoff and active layer deepening can increase DOC and alter DOM composition in ice-wedge polygonal tundra ponds, as observed when comparing years with distinct weather patterns. However, N and P did not increase to the same extent as C did during the wet and warm year. This result is intriguing, as it contradicts the expectation that most of the nutrients entering these systems are primarily DOM-related. The discrepancy linked to precipitation change suggests that another component of the terrestrial pool, or within the ponds that are relatively more C-rich, is being mobilized.

The combined increase in precipitation and thawing degree-days in 2019 compared to the previous two years (249 and 459% more precipitation than in 2017 and 2018, respectively, and 143% higher degree-days accumulated by July 15; **Fig. 6**) has influenced DOM inputs and its composition. The higher DOC concentrations observed at the surface of ponds in 2019 could be linked to greater inputs from the watershed, increased permafrost erosion associated with active layer deepening, increased autochthonous production, and more frequent mixing events with deeper DOC-enriched water, potentially driven by rainfall events (Rooney et al., 2018). Studies have already linked changes in DOC and DOM quality to the frequency and intensity of rainfall in tundra headwater streams and ponds (Abnizova et al., 2014; Fouché et al., 2017; Coch et al., 2019). These conditions increase the lateral transfer of solutes to ponds, mobilizing DOM and inorganic nutrients from deeper soils, including permafrost-derived materials, and could stimulate the production of cyanobacterial mats in the ponds. This might explain the observed changes in DOM optical properties, particularly the greater contribution of component HT4 (characteristic of cyanobacterial mat leachates) and HM2 (characteristic of the transition layer and permafrost leachates; **Fig. 4**).

The predicted warmer and wetter conditions in the Arctic will have different consequences for organic matter cycling, depending on whether the dominant source is primary producers or permafrost soils. While the microbial and photochemical degradation of excess DOM leached from thawing permafrost soils could lead to increased emissions of old carbon (^{14}C-depleted) to the atmosphere, the processing of DOM originating from plants and aquatic producers would recycle recently fixed carbon from the atmosphere.

534 Monitoring trends in water quality will become increasingly important in Arctic watersheds, as factors
535 other than permafrost erosion can affect DOM inputs to freshwater systems.

Acknowledgements

We gratefully thank V. Prėskienis for his assistance in the field in 2018 and for providing data from the leachate incubations. Our appreciation also goes to V. Laderrière and J. Comte for conducting field work in 2019, and to J. Perreault and V. Laderrière for their expertise in the lab. We would like to thank E. Lévesque for her help in identifying the plant communities surrounding the studied ponds, M. Wauthy for his assistance with PARAFAC analysis, and J.F. Lapierre for his valuable input in improving the manuscript. We are grateful to the associate editor of Arctic Science, J. Fouché, and the two anonymous reviewers for their insightful comments and feedback. We also acknowledge the Centre for Northern Studies (CEN) for providing access to research infrastructure and local meteorological data, as well as Parks Canada and the community of Mittimatalik for granting access to the study site. Our thanks go to the Interuniversity Research Group in Limnology (GRIL) for providing access to their analytical services. This work was carried out in the traditional territories of the Inuit, Nunangat.

Author contributions

Conceptualization: TP, IL, MR

Data curation: TP

Formal analysis: TP

Funding acquisition: IL, MR

Investigation: TP, FM, IL

Methodology: TP, FM, IL, RM

Project administration: IL

Resources: TP, IL, MR

Software: TP

Supervision: IL

Validation: TP

Visualization: TP

Writing – original draft: TP

Writing – review & editing: TP, FM, IL, RM, MR

Competing interests

The authors declare there are no competing interests.

Funding statement

This research was supported by the Natural sciences and engineering research council of Canada (Discovery and Northern Supplement grants to IL, CREATE EnviroNorth scholarship to TP), and the Polar Continental Shelf Program (Natural Resources Canada).

Data availability

Data are available in the Nordicana D repository (doi: 10.5885/45894CE-B3C95FF767D14B50) at the following link: https://nordicana.cen.ulaval.ca/dpage.aspx?doi=45894CE-B3C95FF767D14B50.

References

Abnizova, A., Siemens, J., Langer, M., Boike, J. 2012. Small ponds with major impact: The relevance of ponds and lakes in permafrost landscapes to carbon dioxide emissions. Global Biogeochemical Cycles 26. doi:10.1029/2011GB004237.

Abnizova, A., Young, K.L., Lafrenière, M.J. 2014. Pond hydrology and dissolved carbon dynamics at Polar Bear Pass wetland, Bathurst Island, Nunavut, Canada. Ecohydrology 7, 73–90. doi:10.1002/eco.1323.

Allain, A., Alexis, M.A., Bridoux, M.C., Humbert, G., Agnan, Y., Rouelle, M. 2023. Fingerprinting the elemental composition and chemodiversity of vegetation leachates: consequences for dissolved organic matter dynamics in Arctic environments. Biogeochemistry 164, 73–98. doi:10.1007/s10533-022-00925-9.

Allard, M., Sarrazin, D., l'Hérault, E. 2024. Borehole and near-surface ground temperatures in northeastern Canada. doi:10.5885/45291SL-34F28A9491014AFD.

Allesson, L., Andersen, T., Dörsch, P., Eiler, A., Wei, J., Hessen, D.O. 2020. Phosphorus Availability Promotes Bacterial DOC-Mineralization, but Not Cumulative CO2-Production. Frontiers in Microbiology 11. doi:10.3389/fmicb.2020.569879.

Anderson, N.J., Stedmon, C.A. 2007. The effect of evapoconcentration on dissolved organic carbon concentration and quality in lakes of SW Greenland. Freshwater Biology 52, 280–289. doi:10.1111/j.1365-2427.2006.01688.x.

Antoniades, D., Douglas, M.S.V.S. 2003. Comparative physical and chemical limnology of two Canadian High Arctic regions: Alert (Ellesmere Island, NU) and Mould Bay (Prince Patrick Island, NWT). Archiv fur hydrobiologie 158, 485–516. doi:10.1127/0003-9136/2003/0158-0485.

Arsenault, J., Talbot, J., Brown, L.E., Holden, J., Martinez-Cruz, K., Sepulveda-Jauregui, A., Swindles, G.T., Wauthy, M., Lapierre, J.-F. 2022. Biogeochemical Distinctiveness of Peatland Ponds, Thermokarst

Waterbodies, and Lakes. Geophysical Research Letters 49, e2021GL097492. doi:10.1029/2021GL097492.

Bahram, M., Bro, R., Stedmon, C., Afkhami, A. 2006. Handling of Rayleigh and Raman scatter for PARAFAC modeling of fluorescence data using interpolation. Journal of Chemometrics 20, 99–105. doi:10.1002/cem.978.

Beel, C.R., Heslop, J.K., Orwin, J.F., Pope, M.A., Schevers, A.J., Hung, J.K.Y., Lafrenière, M.J., Lamoureux, S.F. 2021. Emerging dominance of summer rainfall driving High Arctic terrestrial-aquatic connectivity. Nature Communications 12, 1448. doi:10.1038/s41467-021-21759-3.

Beermann, F., Langer, M., Wetterich, S., Strauss, J., Boike, J., Fiencke, C., Schirrmeister, L., Pfeiffer, E.-M., Kutzbach, L. 2017. Permafrost Thaw and Liberation of Inorganic Nitrogen in Eastern Siberia. Permafrost and Periglacial Processes 28, 605–618. doi:10.1002/ppp.1958.

Benner, R. 2003. 5 - Molecular Indicators of the Bioavailability of Dissolved Organic Matter, in: Findlay, S.E.G., Sinsabaugh, R.L. (Eds.), Aquatic Ecosystems, Aquatic Ecology. Academic Press, Burlington, pp. 121–137. doi:10.1016/B978-012256371-3/50006-8.

Berggren, M., del Giorgio, P.A. 2015. Distinct patterns of microbial metabolism associated to riverine dissolved organic carbon of different source and quality. Journal of Geophysical Research: Biogeosciences 120, 989–999. doi:10.1002/2015JG002963.

Berggren, M., Laudon, H., Jansson, M. 2007. Landscape regulation of bacterial growth efficiency in boreal freshwaters. Global Biogeochemical Cycles 21. doi:10.1029/2006GB002844.

Bintanja, R. 2018. The impact of Arctic warming on increased rainfall. Scientific Reports 8, 16001. doi:10.1038/s41598-018-34450-3.

Bittar, T.B., Vieira, A.A.H., Stubbins, A., Mopper, K. 2015. Competition between photochemical and biological degradation of dissolved organic matter from the cyanobacteria Microcystis aeruginosa. Limnology and Oceanography 60, 1172–1194. doi:10.1002/lno.10090.

Breton, J., Vallières, C., Laurion, I. 2009. Limnological properties of permafrost thaw ponds in northeastern Canada. Canadian Journal of Fisheries and Aquatic Sciences. 66, 1635–1648. doi:10.1139/F09-108.

Broek, T.A.B., McCarthy, M.D., Ianiri, H.L., Vaughn, J.S., Mason, H.E., Knapp, A.N. 2023. Dominant heterocyclic composition of dissolved organic nitrogen in the ocean: A new paradigm for cycling and persistence. Proceedings of the National Academy of Sciences 120, e2305763120. doi:10.1073/pnas.2305763120.

628 Catalán, N., Marcé, R., Kothawala, D.N., Tranvik, L.J. 2016. Organic carbon decomposition rates
629 controlled by water retention time across inland waters. Nature Geoscience 9, 501–504.
630 doi:10.1038/ngeo2720.
631 CEN, 2020. Climate station data from Bylot Island in Nunavut, Canada. doi:10.5885/45039SL-
632 EE76C1BDAADC4890.
633 Chen, M., Jaffé, R. 2014. Photo- and bio-reactivity patterns of dissolved organic matter from biomass and
634 soil leachates and surface waters in a subtropical wetland. Water Research 61, 181–190.
635 doi:10.1016/j.watres.2014.03.075.
636 Cherrier, J., Bauer, J.E. 2004. Bacterial utilization of transient plankton-derived dissolved organic carbon
637 and nitrogen inputs in surface ocean waters. Aquatic Microbial Ecology 35, 229–241.
638 doi:10.3354/ame035229.
639 Coch, C., Juhls, B., Lamoureux, S.F., Lafrenière, M.J., Fritz, M., Heim, B., Lantuit, H. 2019. Comparisons of
640 dissolved organic matter and its optical characteristics in small low and high Arctic catchments.
641 Biogeosciences 16, 4535–4553. doi:10.5194/bg-16-4535-2019.
642 Coch, C., Ramage, J.L., Lamoureux, S.F., Meyer, H., Knoblauch, C., Lantuit, H. 2020. Spatial Variability of
643 Dissolved Organic Carbon, Solutes, and Suspended Sediment in Disturbed Low Arctic Coastal
644 Watersheds. Journal of Geophysical Research: Biogeosciences 125, e2019JG005505.
645 doi:10.1029/2019JG005505.
646 Côté, G., Pienitz, R., Velle, G., Wang, X. 2010. Impact of Geese on the Limnology of Lakes and Ponds from
647 Bylot Island (Nunavut, Canada). International Review of Hydrobiology 95, 105–129.
648 doi:10.1002/iroh.200911151.
649 Coulombe, S., Fortier, D., Bouchard, F., Paquette, M., Charbonneau, S., Lacelle, D., Laurion, I., Pienitz, R.
650 2022. Contrasted geomorphological and limnological properties of thermokarst lakes formed in
651 buried glacier ice and ice-wedge polygon terrain. The Cryosphere 16, 2837–2857. doi:10.5194/tc-16-
652 2837-2022.
653 Dixon, P. 2003. VEGAN, a package of R functions for community ecology. Journal of Vegetation Science
654 14, 927–930. doi:10.1111/j.1654-1103.2003.tb02228.x.
655 Dranga, S.A., Hayles, S., Gajewski, K. 2018. Synthesis of limnological data from lakes and ponds across
656 Arctic and Boreal Canada. Arctic Science 4, 167–185. doi:10.1139/as-2017-0039.
657 Dupont, A., Botrel, M., St-Gelais, N.F., Poisot, T., Maranger, R. 2023. A social–ecological geography of
658 southern Canadian lakes. FACETS 8, 1–16. doi:10.1139/facets-2023-0025.

659 Fortier, D., Allard, M. 2004. Late Holocene syngenetic ice-wedge polygons development, Bylot Island,
660 Canadian Arctic Archipelago. Canadian Journal of Earth Sciences 41, 997–1012. doi:10.1139/e04-031.
661 Fouché, J., Lafrenière, M.J., Rutherford, K., Lamoureux, S. 2017. Seasonal hydrology and permafrost
662 disturbance impacts on dissolved organic matter composition in High Arctic headwater catchments.
663 Arctic Science 3, 378–405. doi:10.1139/as-2016-0031.
664 Fouché, J., Christiansen, C.T., Lafrenière, M.J., Grogan, P., Lamoureux, S.F. 2020. Canadian permafrost
665 stores large pools of ammonium and optically distinct dissolved organic matter. Nature
666 Communications 11, 4500. doi :10.1038/s41467-020-18331-w.
667 Franke, D., Hamilton, M.W., Ziegler, S.E. 2012. Variation in the photochemical lability of dissolved organic
668 matter in a large boreal watershed. Aquatic Sciences 74, 751–768. doi:10.1007/s00027-012-0258-3.
669 Grosse, G., Jones, B.M., Arp, C.D. 2013. Thermokarst lakes, drainage, and drained basins, in: Treatise on
670 Geomorphology. pp. 325–353. doi:10.1016/B978-0-12-374739-6.00216-5.
671 Hamdan, M., Byström, P., Hotchkiss, E.R., Al-Haidarey, M.J., Karlsson, J. 2021. An experimental test of
672 climate change effects in northern lakes: Increasing allochthonous organic matter and warming alters
673 autumn primary production. Freshwater Biology 66, 815–825. doi:10.1111/fwb.13679.
674 Harrell, F.E. 2024. Hmisc: Harrell Miscellaneous. _Hmisc: Harrell Miscellaneous_. R package version 5.1-3,
675 <https://hbiostat.org/R/Hmisc/>.
676 Helms, J.R., Stubbins, A., Ritchie, J.D., Minor, E.C., Kieber, D.J., Mopper, K. 2008. Absorption spectral
677 slopes and slope ratios as indicators of molecular weight, source, and photobleaching of
678 chromophoric dissolved organic matter. Limnology and Oceanography 53, 955–969.
679 doi:10.4319/lo.2008.53.3.0955.
680 Ianiri, H.L., McCarthy, M.D. 2023. Compound specific δ15N analysis of amino acids reveals unique
681 sources and differential cycling of high and low molecular weight marine dissolved organic nitrogen.
682 Geochimica et Cosmochimica Acta 344, 24–39. doi:10.1016/j.gca.2023.01.008.
683 Jorgenson, M.T., Kanevskiy, M., Shur, Y., Moskalenko, N., Brown, D.R.N., Wickland, K., Striegl, R., Koch, J.
684 2015. Role of ground ice dynamics and ecological feedbacks in recent ice wedge degradation and
685 stabilization. Journal of Geophysical Research: Earth Surface 120, 2280–2297.
686 doi:10.1002/2015JF003602.
687 Kanevskiy, M., Shur, Y., Jorgenson, M.T., Ping, C.-L., Michaelson, G.J., Fortier, D., Stephani, E., Dillon, M.,
688 Tumskoy, V. 2013. Ground ice in the upper permafrost of the Beaufort Sea coast of Alaska. Cold
689 Regions Science and Technology 85, 56–70. doi:10.1016/j.coldregions.2012.08.002.

690 Kartoziia, A. 2019. Assessment of the Ice Wedge Polygon Current State by Means of UAV Imagery
691 Analysis (Samoylov Island, the Lena Delta). Remote Sensing 11, 1627. doi:10.3390/rs11131627.
692 Kassambara, A. 2023. _rstatix: Pipe-Friendly Framework for Basic Statistical Tests_. R package version
693 0.7.2, <https://rpkgs.datanovia.com/rstatix/>.
694 Kellerman, A.M., Kothawala, D.N., Dittmar, T., Tranvik, L.J. 2015. Persistence of dissolved organic matter
695 in lakes related to its molecular characteristics. Nature Geoscience 8, 454–457.
696 doi:10.1038/ngeo2440.
697 Koch, J.C., Gurney, K., Wipfli, M.S. 2014. Morphology-Dependent Water Budgets and Nutrient Fluxes in
698 Arctic Thaw Ponds. Permafrost and Periglacial Processes 25, 79–93. doi:10.1002/ppp.1804.
699 Kokelj, S.V., Lantz, T.C., Wolfe, S.A., Kanigan, J.C., Morse, P.D., Coutts, R., Molina-Giraldo, N., Burn, C.R.
700 2014. Distribution and activity of ice wedges across the forest-tundra transition, western Arctic
701 Canada. Journal of Geophysical Research: Earth Surface 119, 2032–2047. doi:10.1002/2014JF003085.
702 Kopyrina, L., Pshennikova, E., Barinova, S. 2020. Diversity and ecological characteristic of algae and
703 cyanobacteria of thermokarst lakes in Yakutia (northeastern Russia). Oceanological and
704 Hydrobiological Studies 49, 99–122. doi:10.1515/ohs-2020-0010.
705 Kothawala, D.N., Kellerman, A.M., Catalán, N., Tranvik, L.J. 2021. Organic Matter Degradation across
706 Ecosystem Boundaries: The Need for a Unified Conceptualization. Trends in Ecology & Evolution 36,
707 113–122. doi:10.1016/j.tree.2020.10.006.
708 Lafrenière, M.J., Lamoureux, S.F. 2013. Thermal Perturbation and Rainfall Runoff have Greater Impact on
709 Seasonal Solute Loads than Physical Disturbance of the Active Layer. Permafrost and Periglacial
710 Processes 24, 241–251. doi:10.1002/ppp.1784.
711 Lamoureux, S.F., Lafrenière, M.J. 2014. Seasonal fluxes and age of particulate organic carbon exported
712 from Arctic catchments impacted by localized permafrost slope disturbances. Environmental
713 Research Letters 9, 045002. doi:10.1088/1748-9326/9/4/045002.
714 Langer, M., Westermann, S., Walter Anthony, K., Wischnewski, K., Boike, J. 2015. Frozen ponds:
715 production and storage of methane during the Arctic winter in a lowland tundra landscape in
716 northern Siberia, Lena River delta. Biogeosciences 12, 977–990. doi:10.5194/bg-12-977-2015.
717 Lara, M.J., McGuire, A.D., Euskirchen, E.S., Tweedie, C.E., Hinkel, K.M., Skurikhin, A.N., Romanovsky, V.E.,
718 Grosse, G., Bolton, W.R., Genet, H. 2015. Polygonal tundra geomorphological change in response to
719 warming alters future CO2 and CH4 flux on the Barrow Peninsula. Global Change Biology 21, 1634–
720 1651. doi:10.1111/gcb.12757.

721 Lara, M.J., McGuire, A.D., Euskirchen, E.S., Genet, H., Yi, S., Rutter, R., Iversen, C., Sloan, V., Wullschleger,
722 S.D. 2020. Local-scale Arctic tundra heterogeneity affects regional-scale carbon dynamics. Nature
723 Communications 11, 4925. doi:10.1038/s41467-020-18768-z.
724 Laurion, I., Mladenov, N. 2013. Dissolved organic matter photolysis in Canadian arctic thaw ponds.
725 Environmental Research Letters 8, 035026. doi:10.1088/1748-9326/8/3/035026.
726 Liljedahl, A.K., Boike, J., Daanen, R.P., Fedorov, A.N., Frost, G.V., Grosse, G., Hinzman, L.D., Iijma, Y.,
727 Jorgenson, J.C., Matveyeva, N., Necsoiu, M., Raynolds, M.K., Romanovsky, V.E., Schulla, J., Tape, K.D.,
728 Walker, D.A., Wilson, C.J., Yabuki, H., Zona, D. 2016. Pan-Arctic ice-wedge degradation in warming
729 permafrost and its influence on tundra hydrology. Nature Geoscience 9, 312–318.
730 doi:10.1038/ngeo2674.
731 Lim, D.S.S., Douglas, M.S.V., Smol, J.P., Lean, D.R.S. 2001. Physical and Chemical Limnological
732 Characteristics of 38 Lakes and Ponds on Bathurst Island, Nunavut, Canadian High Arctic. International
733 Review of Hydrobiology 86, 1–22. doi:10.1002/1522-2632(200101)86:1<1::AID-IROH1>3.0.CO;2-E.
734 Ma, Q., Jin, H., Yu, C., Bense, V.F. 2019. Dissolved organic carbon in permafrost regions: A review. Science
735 China Earth Science 62, 349–364. doi:10.1007/s11430-018-9309-6.
736 Maechler, M., Rousseeuw, P., Struyf, A., Hubert, M., Hornik, K. 2023. cluster: Cluster Analysis Basics and
737 Extensions. R package version 2.1.6.
738 Magnússon, R.Í., Limpens, J., van Huissteden, J., Kleijn, D., Maximov, T.C., Rotbarth, R., Sass-Klaassen, U.,
739 Heijmans, M.M.P.D. 2020. Rapid Vegetation Succession and Coupled Permafrost Dynamics in Arctic
740 Thaw Ponds in the Siberian Lowland Tundra. Journal of Geophysical Research: Biogeosciences 125,
741 e2019JG005618. doi:10.1029/2019JG005618.
742 Maranger, R., Pullin, M.J. 2003. Elemental Complexation by Dissolved Organic Matter in Lakes:
743 Implications for Fe Speciation and the Speciation and the Bioavailability of Fe and P, in: Findlay, S.E.G.,
744 Sinsabaugh, R.L. (Eds.), Aquatic Ecosystems, Aquatic Ecology. Academic Press, Burlington, pp. 185–
745 214. doi:10.1016/B978-012256371-3/50009-3.
746 Maranger, R., Jones, S.E., Cotner, J.B. 2018. Stoichiometry of carbon, nitrogen, and phosphorus through
747 the freshwater pipe. Limnology and Oceanography Letters 3, 89–101. doi:10.1002/lol2.10080.
748 Mariash, H.L., Smith, P.A., Mallory, M. 2018. Decadal Response of Arctic Freshwaters to Burgeoning
749 Goose Populations. Ecosystems 21, 1230–1243. doi:10.1007/s10021-017-0215-z.
750 Martin, A.F., Lantz, T.C., Humphreys, E.R. 2018. Ice wedge degradation and CO2 and CH4 emissions in the
751 Tuktoyaktuk Coastlands, Northwest Territories. Arctic Science 4, 130–145. doi:10.1139/as-2016-0011.

752 Matveev, A., Laurion, I., Deshpande, B.N., Bhiry, N., Vincent, W.F. 2016. High methane emissions from
753 thermokarst lakes in subarctic peatlands. Limnology and Oceanography 61, S150–S164.
754 doi:10.1002/lno.10311.
755 Matveev, A., Laurion, I., Vincent, W.F. 2019. Winter Accumulation of Methane and its Variable Timing of
756 Release from Thermokarst Lakes in Subarctic Peatlands. Journal of Geophysical Research:
757 Biogeosciences 124, 3521–3535. doi:10.1029/2019JG005078.
758 Mazoyer, F. 2023. La dégradation photochimique et biologique de la matière organique dissoute
759 provenant de mares thermokarstiques et de sources terrestres des paysages de pergélisol arctique de
760 l'est du Canada / Photochemical and biological degradation of dissolved organic matter from
761 thermokarst ponds and terrestrial sources in arctic permafrost landscapes of eastern Canada. (phd).
762 Doctorat en sciences de l'eau, Québec.
763 McKnight, D.M., Boyer, E.W., Westerhoff, P.K., Doran, P.T., Kulbe, T., Andersen, D.T. 2001.
764 Spectrofluorometric characterization of dissolved organic matter for indication of precursor organic
765 material and aromaticity. Limnology and Oceanography 46, 38–48. doi:10.4319/lo.2001.46.1.0038.
766 Mekonnen, Z.A., Riley, W.J., Berner, L.T., Bouskill, N.J., Torn, M.S., Iwahana, G., Breen, A.L., Myers-Smith,
767 I.H., Criado, M.G., Liu, Y., Euskirchen, E.S., Goetz, S.J., Mack, M.C., Grant, R.F. 2021. Arctic tundra
768 shrubification: a review of mechanisms and impacts on ecosystem carbon balance. Environmental
769 Research Letters 16, 053001. doi :10.1088/1748-9326/abf28b.
770 Mostovaya, A., Koehler, B., Guillemette, F., Brunberg, A.-K., Tranvik, L.J. 2016. Effects of compositional
771 changes on reactivity continuum and decomposition kinetics of lake dissolved organic matter. Journal
772 of Geophysical Research: Biogeosciences 121, 1733–1746. doi:10.1002/2016JG003359.
773 Murphy, K.R. 2011. A Note on Determining the Extent of the Water Raman Peak in Fluorescence
774 Spectroscopy. Applied Spectroscopy 65, 233–236. doi:10.1366/10-06136.
775 Murphy, K., Stedmon, C., Wenig, P., Bro, R. 2014. OpenFluor– an online spectral library of auto-
776 fluorescence by organic compounds in the environment. Analytical Methods 6, 658–661.
777 doi:10.1039/C3AY41935E.
778 Murphy, K.R., Timko, S.A., Gonsior, M., Powers, L.C., Wünsch, U.J., Stedmon, C.A. 2018. Photochemistry
779 Illuminates Ubiquitous Organic Matter Fluorescence Spectra. Environmental Science & Technology
780 52, 11243–11250. doi :10.1021/acs.est.8b02648.
781 Muster, S., Roth, K., Langer, M., Lange, S., Cresto Aleina, F., Bartsch, A., Morgenstern, A., Grosse, G.,
782 Jones, B., Sannel, A.B.K., Sjöberg, Y., Günther, F., Andresen, C., Veremeeva, A., Lindgren, P.R.,
783 Bouchard, F., Lara, M.J., Fortier, D., Charbonneau, S., Virtanen, T.A., Hugelius, G., Palmtag, J., Siewert,

784 M.B., Riley, W.J., Koven, C.D., Boike, J. 2017. PeRL: a circum-Arctic Permafrost Region Pond and Lake
785 database. Earth System Science Data 9, 317–348. doi:10.5194/essd-9-317-2017.
786 Niedrist, G.H., Psenner, R., Sommaruga, R. 2018. Climate warming increases vertical and seasonal water
787 temperature differences and inter-annual variability in a mountain lake. Climatic Change 151, 473–
788 490. doi:10.1007/s10584-018-2328-6.
789 Obu, J., Westermann, S., Bartsch, A., Berdnikov, N., Christiansen, H.H., Dashtseren, A., Delaloye, R.,
790 Elberling, B., Etzelmüller, B., Kholodov, A., Khomutov, A., Kääb, A., Leibman, M.O., Lewkowicz, A.G.,
791 Panda, S.K., Romanovsky, V., Way, R.G., Westergaard-Nielsen, A., Wu, T., Yamkhin, J., Zou, D. 2019.
792 Northern Hemisphere permafrost map based on TTOP modelling for 2000–2016 at 1 km2 scale. Earth-
793 Science Reviews 193, 299–316. doi:10.1016/j.earscirev.2019.04.023.
794 Ola, A., Fortier, D., Coulombe, S., Comte, J., Domine, F. 2022. The Distribution of Soil Carbon and
795 Nitrogen Stocks Among Dominant Geomorphological Terrain Units in Qarlikturvik Valley, Bylot Island,
796 Arctic Canada. Journal of Geophysical Research: Biogeosciences 127, e2021JG006750.
797 doi:10.1029/2021JG006750.
798 Pilla, R.M., Williamson, C.E., Zhang, J., Smyth, R.L., Lenters, J.D., Brentrup, J.A., Knoll, L.B., Fisher, T.J.
799 2018. Browning-Related Decreases in Water Transparency Lead to Long-Term Increases in Surface
800 Water Temperature and Thermal Stratification in Two Small Lakes. Journal of Geophysical Research:
801 Biogeosciences 123, 1651–1665. doi:10.1029/2017JG004321.
802 Poulin, B.A., Ryan, J.N., Aiken, G.R. 2014. Effects of Iron on Optical Properties of Dissolved Organic
803 Matter. Environmental Science & Technology 48, 10098–10106. doi :10.1021/es502670r.
804 Prėskienis, V. 2022. La forte variabilité des émissions de gaz à effet de serre des lacs et des mares de
805 l'Arctique expliquée par la morphologie des plans d'eau, l'activité érosive et la qualité de la matière
806 organique des sols environnants. / The high variability of greenhouse gas emissions from Arctic lakes
807 and ponds explained by the morphology of water bodies, the erosional activity and the quality of
808 organic matter in surrounding soils. (phd). Institut National de la Recherche Scientifique, Québec.
809 Prėskienis, V., Laurion, I., Bouchard, F., Douglas, P.M.J., Billett, M.F., Fortier, D., Xu, X. 2021. Seasonal
810 patterns in greenhouse gas emissions from lakes and ponds in a High Arctic polygonal landscape.
811 Limnology and Oceanography 66, S117–S141. doi:10.1002/lno.11660.
812 R Core Team, 2024. _R: A Language and Environment for Statistical Computing_. R Foundation for
813 Statistical Computing.
814 Rautio, M., Dufresne, F., Laurion, I., Bonilla, S., Vincent, W.F., Christoffersen, K.S. 2011. Shallow
815 freshwater ecosystems of the circumpolar Arctic. Écoscience. doi:10.2980/18-3-3463.

816 Raynolds, M.K., Walker, D.A., Ambrosius, K.J., Brown, J., Everett, K.R., Kanevskiy, M., Kofinas, G.P.,
817 Romanovsky, V.E., Shur, Y., Webber, P.J. 2014. Cumulative geoecological effects of 62 years of
818 infrastructure and climate change in ice-rich permafrost landscapes, Prudhoe Bay Oilfield, Alaska.
819 Global Change Biology 20, 1211–1224. doi:10.1111/gcb.12500.
820 Reed, A., Hughes, R.J., Boyd, H. 2002. Patterns of distribution and abundance of Greater Snow Geese on
821 Bylot Island, Nunavut, Canada 1983-1998. Wildfowl 53, 53–65.
822 Rioux, K. 2020. Impacts de la dégradation du pergélisol par thermo-érosion sur les processus
823 hydrologiques et les flux de matières (masters). Université de Montréal, Montréal.
824 Roiha, T., Laurion, I., Rautio, M. 2015. Carbon dynamics in highly heterotrophic subarctic thaw ponds.
825 Biogeosciences 12, 7223–7237. doi:10.5194/bg-12-7223-2015.
826 Rooney, G.G., van Lipzig, N., Thiery, W. 2018. Estimating the effect of rainfall on the surface temperature
827 of a tropical lake. Hydrology and Earth System Sciences 22, 6357–6369. doi:10.5194/hess-22-6357-
828 2018.
829 Saros, J.E., Arp, C.D., Bouchard, F., Comte, J., Couture, R.-M., Dean, J.F., Lafrenière, M., MacIntyre, S.,
830 McGowan, S., Rautio, M., Prater, C., Tank, S.E., Walvoord, M., Wickland, K.P., Antoniades, D., Ayala-
831 Borda, P., Canario, J., Drake, T.W., Folhas, D., Hazuková, V., Kivilä, H., Klanten, Y., Lamoureux, S.,
832 Laurion, I., Pilla, R.M., Vonk, J.E., Zolkos, S., Vincent, W.F. 2023. Sentinel responses of Arctic
833 freshwater systems to climate: linkages, evidence, and a roadmap for future research. Arctic Science
834 9, 356–392. doi:10.1139/as-2022-0021.
835 Schuur, E.A.G., Abbott, B.W., Commane, R., Ernakovich, J., Euskirchen, E., Hugelius, G., Grosse, G., Jones,
836 M., Koven, C., Leshyk, V., Lawrence, D., Loranty, M.M., Mauritz, M., Olefeldt, D., Natali, S.,
837 Rodenhizer, H., Salmon, V., Schädel, C., Strauss, J., Treat, C., Turetsky, M. 2022. Permafrost and
838 Climate Change: Carbon Cycle Feedbacks From the Warming Arctic. Annual Review of Environment
839 and Resources 47, 343–371. doi:10.1146/annurev-environ-012220-011847.
840 Sipler, R.E., Bronk, D.A. 2015. Chapter 4 - Dynamics of Dissolved Organic Nitrogen, in: Hansell, D.A.,
841 Carlson, C.A. (Eds.), Biogeochemistry of Marine Dissolved Organic Matter (Second Edition). Academic
842 Press, Boston, pp. 127–232. doi:10.1016/B978-0-12-405940-5.00004-2.
843 Sobek, S., Tranvik, L.J., Prairie, Y.T., Kortelainen, P., Cole, J.J. 2007. Patterns and regulation of dissolved
844 organic carbon: An analysis of 7,500 widely distributed lakes. Limnology and Oceanography 52, 1208–
845 1219. doi:10.4319/lo.2007.52.3.1208.

Spencer, R.G.M., Mann, P.J., Dittmar, T., Eglinton, T.I., McIntyre, C., Holmes, R.M., Zimov, N., Stubbins, A. 2015. Detecting the signature of permafrost thaw in Arctic rivers. Geophysical Research Letters 42, 2830–2835. doi:10.1002/2015GL063498.

Stedmon, C.A., Markager, S., Bro, R. 2003. Tracing dissolved organic matter in aquatic environments using a new approach to fluorescence spectroscopy. Marine Chemistry 82, 239–254. doi:10.1016/S0304-4203(03)00072-0.

Stolpmann, L., Coch, C., Morgenstern, A., Boike, J., Fritz, M., Herzschuh, U., Stoof-Leichsenring, K., Dvornikov, Y., Heim, B., Lenz, J., Larsen, A., Walter Anthony, K., Jones, B., Frey, K., Grosse, G. 2021. First pan-Arctic assessment of dissolved organic carbon in lakes of the permafrost region. Biogeosciences 18, 3917–3936. doi:10.5194/bg-18-3917-2021.

Sundman, A., Karlsson, T., Sjöberg, S., Persson, P. 2016. Impact of iron–organic matter complexes on aqueous phosphate concentrations. Chemical Geology 426, 109–117. doi:10.1016/j.chemgeo.2016.02.008.

Tank, S.E., Vonk, J.E., Walvoord, M.A., McClelland, J.W., Laurion, I., Abbott, B.W. 2020. Landscape matters: Predicting the biogeochemical effects of permafrost thaw on aquatic networks with a state factor approach. Permafrost and Periglacial Processes 31, 358–370. doi:10.1002/ppp.2057.

Textor, S.R., Wickland, K.P., Podgorski, D.C., Johnston, S.E., Spencer, R.G.M. 2019. Dissolved Organic Carbon Turnover in Permafrost-Influenced Watersheds of Interior Alaska: Molecular Insights and the Priming Effect. Frontiers in Earth Science 7. doi:10.3389/feart.2019.00275.

Tremblay, L., Benner, R. 2009. Organic matter diagenesis and bacterial contributions to detrital carbon and nitrogen in the Amazon River system. Limnology and Oceanography 54, 681–691. doi:10.4319/lo.2009.54.3.0681.

Van Geest, G.J., Hessen, D.O., Spierenburg, P., Dahl-Hansen, G.A.P., Christensen, G., Faerovig, P.J., Brehm, M., Loonen, M.J.J.E., Van Donk, E. 2007. Goose-mediated nutrient enrichment and planktonic grazer control in arctic freshwater ponds. Oecologia 153, 653–662. doi:10.1007/s00442-007-0770-7.

Vézina, S., Vincent, W.F. 1997. Arctic cyanobacteria and limnological properties of their environment: Bylot Island, Northwest Territories, Canada (73°N, 80°W). Polar Biology 17, 523–534. doi:10.1007/s003000050151.

Vonk, J.E., Tank, S.E., Bowden, W.B., Laurion, I., Vincent, W.F., Alekseychik, P., Amyot, M., Billet, M.F., Canário, J., Cory, R.M., Deshpande, B.N., Helbig, M., Jammet, M., Karlsson, J., Larouche, J., MacMillan, G., Rautio, M., Walter Anthony, K.M., Wickland, K.P. 2015. Reviews and syntheses: Effects of

permafrost thaw on Arctic aquatic ecosystems. Biogeosciences 12, 7129–7167. doi:10.5194/bg-12-7129-2015.

Wang, Y., Xu, Y., Spencer, R.G.M., Zito, P., Kellerman, A., Podgorski, D., Xiao, W., Wei, D., Rashid, H., Yang, Y. 2018. Selective Leaching of Dissolved Organic Matter From Alpine Permafrost Soils on the Qinghai-Tibetan Plateau. Journal of Geophysical Research: Biogeosciences 123, 1005–1016. doi:10.1002/2017JG004343.

Wauthy, M., Rautio, M. 2020. Emergence of steeply stratified permafrost thaw ponds changes zooplankton ecology in subarctic freshwaters. Arctic, Antarctic, and Alpine Research 52, 177–190. doi:10.1080/15230430.2020.1753412.

Wauthy, M., Rautio, M., Christoffersen, K.S., Forsström, L., Laurion, I., Mariash, H.L., Peura, S., Vincent, W.F. 2018. Increasing dominance of terrigenous organic matter in circumpolar freshwaters due to permafrost thaw. Limnology and Oceanography Letters 3, 186–198. doi:10.1002/lol2.10063.

Weishaar, J.L., Aiken, G.R., Bergamaschi, B.A., Fram, M.S., Fujii, R., Mopper, K. 2003. Evaluation of Specific Ultraviolet Absorbance as an Indicator of the Chemical Composition and Reactivity of Dissolved Organic Carbon. Environmental Science & Technology 37, 4702–4708. doi:10.1021/es030360x.

Wrona, F.J., Johansson, M., Culp, J.M., Jenkins, A., Mård, J., Myers-Smith, I.H., Prowse, T.D., Vincent, W.F., Wookey, P.A. 2016. Transitions in Arctic ecosystems: Ecological implications of a changing hydrological regime. Journal of Geophysical Research: Biogeosciences 121, 650–674. doi:10.1002/2015JG003133.

Table 1. Description of the PARAFAC components based on comparison of excitation and emission spectra against components published in the OpenFluor database (http://www.openfluor.org/; accessed on 4 March 2021) and leachates of potential DOM sources. Brackets for emissions peak indicate the secondary peak maximum.

PARAFAC component	Excitation maxima (nm)	Emission maxima (nm)	Description	Assignment of potential sources based on leachates	Number of OpenFluor matches
HT1 (C1)	<250 (315)	424	Humic-like	Soils, abundant in active layer, transition layer and permafrost	39
HT2 (C2)	<250 (335)	448	Humic-like (fulvic-like)	Soils, abundant in active layer, transition layer and permafrost	24
HT3 (C3)	<250 (385)	510	Humic-like (fulvic-like)	Soils, abundant in active layer, transition layer and permafrost	66
P1 (C4)	280	348	Protein-like (amino acid tryptophan-like)	Living and decomposing plants, abundant in grasses and mosses; cyanobacterial mats	33
HM1 (C5)	<250 (305)	378	Humic-like	Active layer; cyanobacterial mats	1
HM2 (C6)	295	410	Humic-like	Soils, abundant in transition layer and permafrost	5
HT4 (C7)	270 (355)	446	Humic-like	Active layer; cyanobacterial mats	16
P2 (C8)	275	<300	Protein-like (amino-acid tyrosine-like)	Living and decomposing plants, abundant in shrubs; cyanobacterial mats	15

Table 2. Mean (± SE) DOC, TN, TP and elemental ratios at the surface of ponds. Values sharing a common letter within a column between years are not significantly different ($P < 0.05$).

	Pond category	n	DOC (mg L^{-1})	TN (µg L^{-1})	TP (µg L^{-1})	C:N -	C:P -	N:P -
2017	eIWT	5	16.0 ± 0.3	1010 ± 31	43.3 ± 1.9	18.6 ± 0.9	994 ± 56	53.4 ± 2.2
	sIWT	5	12.5 ± 0.7	924 ± 75	28.6 ± 6.1	16.0 ± 1.0	1334 ± 201	84.8 ± 14.0
	CP	5	11.2 ± 1.0	1003 ± 75	25.8 ± 3.0	13.1 ± 0.9	1212 ± 142	91.0 ± 5.9
	All	15	**13.2 ± 0.7^{a}**	**979 ± 35^{a}**	**32.6 ± 3.0^{a}**	**15.9 ± 0.8^{a}**	**1180 ± 87^{a}**	**76.4 ± 6.5^{a}**
2018	eIWT	5	14.4 ± 0.6	875 ± 44	36.3 ± 2.3	19.1 ± 0.5	1058 ± 29	55.4 ± 2.3
	sIWT	5	12.9 ± 0.6	814 ± 51	28.5 ± 1.8	18.6 ± 1.0	1225 ± 97	66.0 ± 4.8
	CP	5	10.6 ± 0.7	825 ± 52	22.2 ± 2.2	15.1 ± 0.3	1311 ± 114	86.8 ± 7.6
	All	15	**12.6 ± 0.6^{a}**	**838 ± 27^{b}**	**29.0 ± 1.9^{a}**	**17.6 ± 0.6^{a}**	**1198 ± 55^{a}**	**69.4 ± 4.5^{a}**
2019	eIWT	8	19.0 ± 0.2	960 ± 12	31.4 ± 2.5	23.1 ± 0.2	1686 ± 136	72.9 ± 5.6
	sIWT	6	17.5 ± 1.3	924 ± 55	24.0 ± 2.2	22.2 ± 1.2	2001 ± 182	92.3 ± 10.7
	CP	6	12.8 ± 0.8	940 ± 44	21.0 ± 2.4	15.8 ± 0.5	1735 ± 211	110.0 ± 12.4
	All	20	**16.7 ± 0.7^{b}**	**943 ± 21^{a}**	**26.0 ± 1.7^{a}**	**20.6 ± 0.8^{b}**	**1795 ± 99^{b}**	**89.7 ± 6.2^{a}**

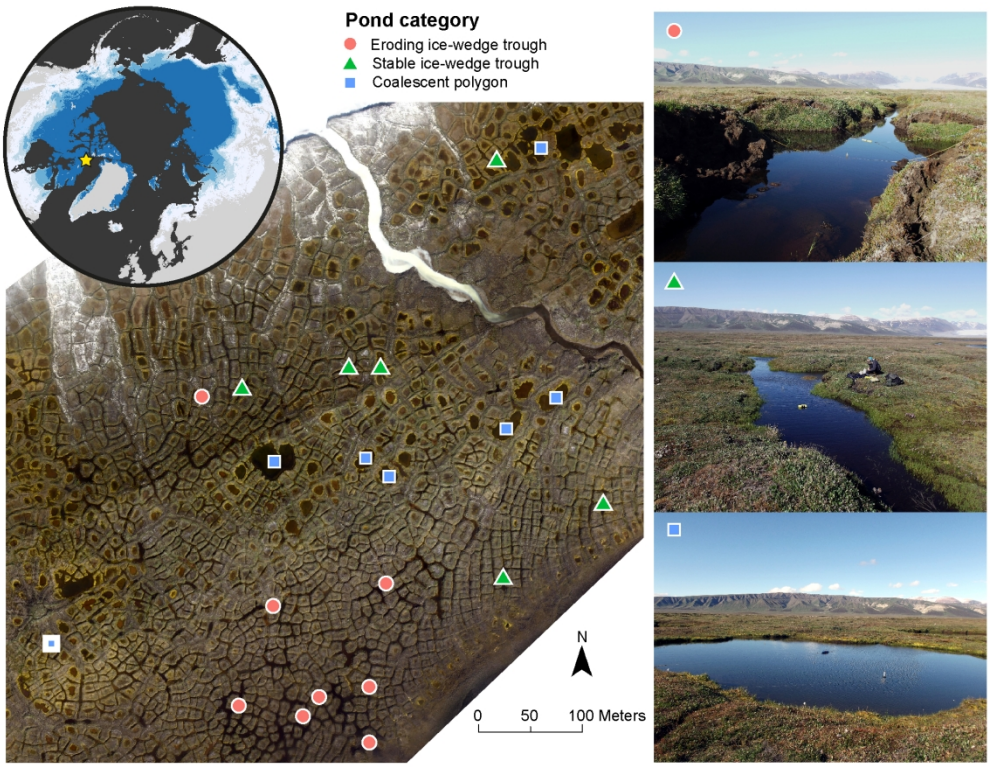

Figure 1. Location of Bylot Island and aerial view of the portion of Qarlikturvik Valley with the sampled ponds. The dark blue area on the inset map (top left) represents the continuous permafrost region. In 2019, all ponds were sampled except for BYL30 (thick white border, in the bottom-left corner). The right panel shows ground-level photographs of archetypal ponds from each category defined in this study, with from top to bottom: eroding ice-wedge trough (eIWT) pond, stable ice-wedge trough (sIWT) pond, and coalescent polygon (CP) pond (© Thomas Pacoureau). Basemap derived from Natural Earth vector data, reprojected to the Arctic polar stereographic projection (EPSG:3995). Permafrost data adapted from Obu et al. (2019). Orthomosaic created using high-resolution photos taken from a helicopter (© Simon Charbonneau).

182x140mm (300 x 300 DPI)

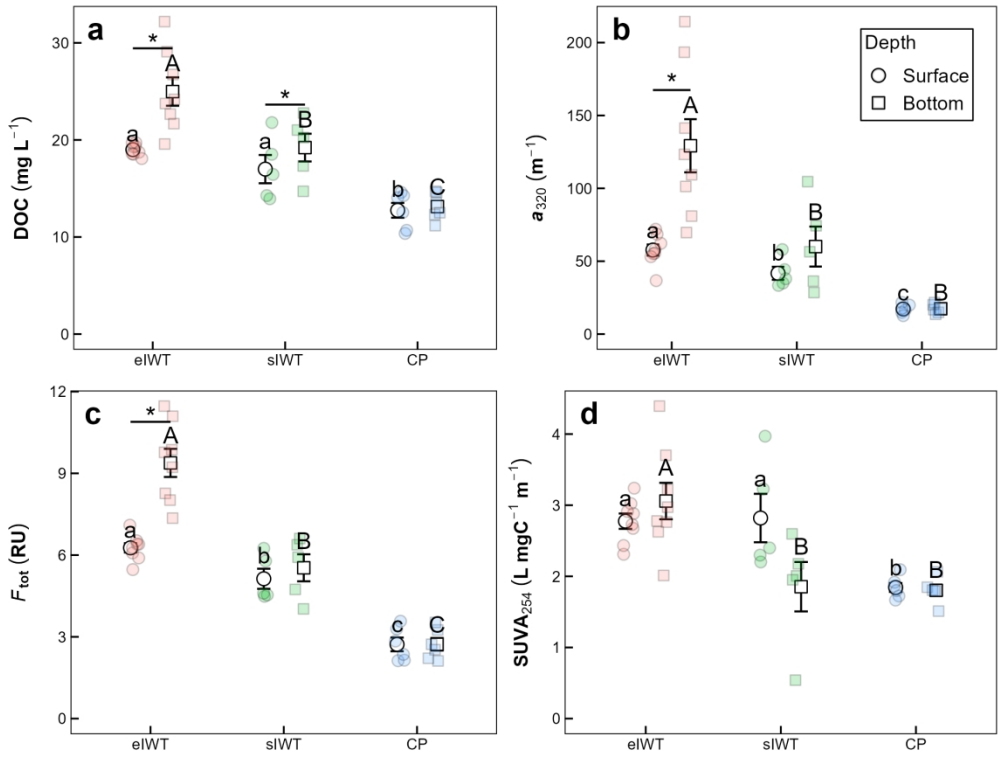

Figure 2. DOC (a), a_{320} (b), F_{tot} (c), and $SUVA_{254}$ (d) in ponds (mean ± SE; eIWT n = 8, sIWT n = 5 and CP n = 6). Differences among pond categories at the same depth and between depths within the same pond category, as determined by post hoc analysis, are indicated by letters or stars, respectively (for $P \leq 0.05$).

181x139mm (300 x 300 DPI)

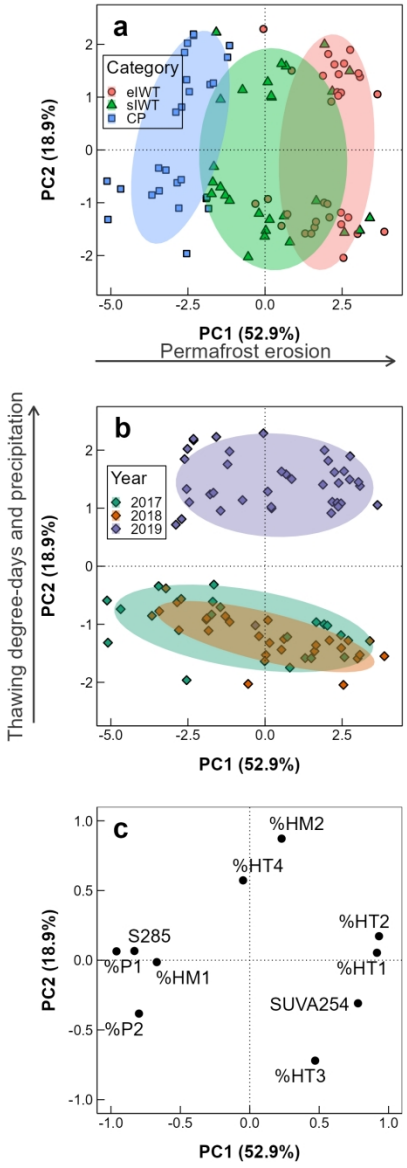

Figure 3. Principal component analysis (PCA) of DOM optical properties in ponds. PCA loading plot for individuals with 68% confidence interval ellipses around the centroid of each pond category (a) or sampling year (b). Loading plot showing the association between variables and the principal components (c). Percent variance explained by each principal component is indicated in brackets on the axis titles. The ellipses for eroding and stable ice-wedge trough ponds intersect, while they show minimal overlap with coalescent polygon ponds.

88x236mm (300 x 300 DPI)

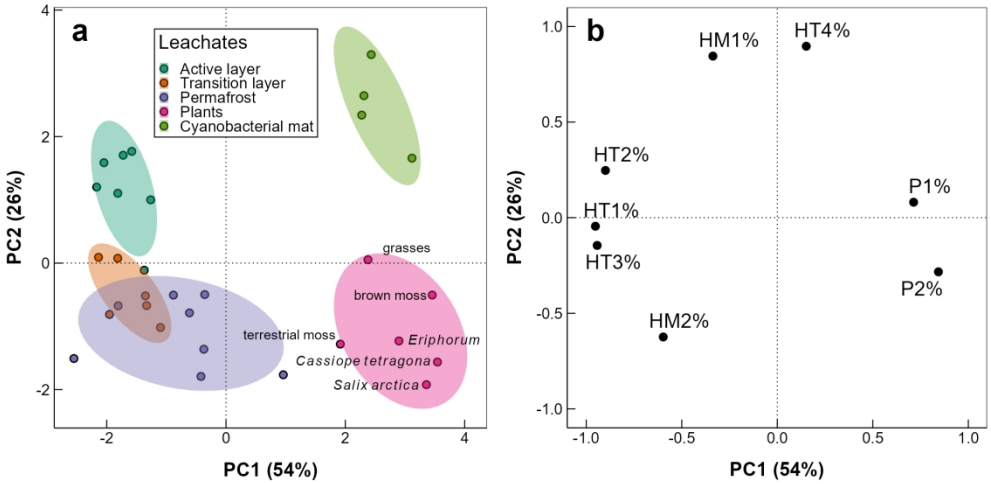

Figure 4. Potential sources of fluorescent DOM in ponds inferred from leachates. Principal component analysis (PCA) loading plot for individuals with 68% confidence interval ellipses around the centroid of each leachate type (a) and loading plot showing the association between variables and the principal components (b). Percent variance explained by each principal component is indicated in brackets on the axis titles.

181x93mm (300 x 300 DPI)

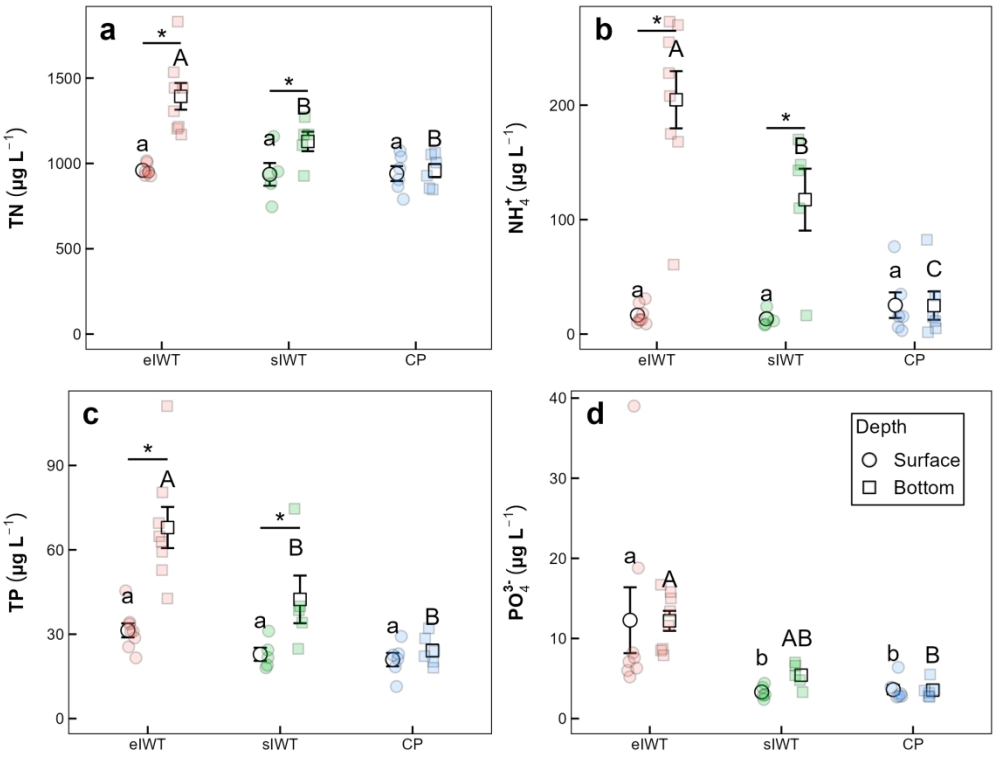

Figure 5. TN (a), NO_3^- (b), NH_4^+ (c), TP (d), and PO_4^{3-} (e) concentrations in ponds (mean ± SE; eIWT: n = 8, sIWT: n = 5, CP: n = 6). Significant differences among pond categories at the same depth and between depths within the same pond category, as determined by post hoc analysis, are indicated by letters or stars, respectively (for $P \leq 0.05$).

181x139mm (300 x 300 DPI)

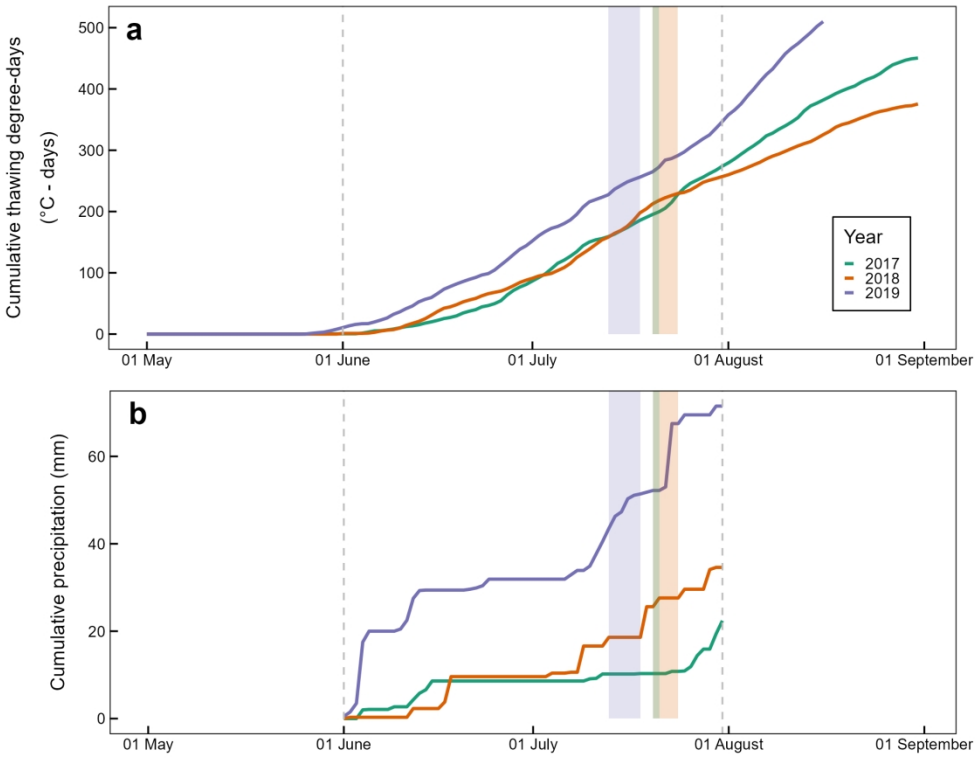

Figure 6. Cumulative thawing degree-days (a) and precipitation (b) at the studied site. Grey dashed lines indicate the precipitation recording period (June 1 to July 31), while air temperature for calculating thawing degree-days was recorded year-round. Shaded areas represent sampling periods, with colours corresponding to the respective years.

181x139mm (300 x 300 DPI)